Металлофиз. новейшие технол. / Metallofiz. Noveishie Tekhnol.
2014, т. 36, № 8, сс. 1091–1099
Оттиски доступны непосредственно от издателя
Фотокопирование разрешено только
в соответствии с лицензией

PACS numbers: 81.05.Bx, 81.07.Bc, 81.07.Wx, 81.20.Ev, 81.30.Kf, 81.30.Mh

Microstructure Investigation of the Spark Plasma Sintered Cu–Al–Ni Shape Memory Material

G. E. Monastyrsky[*,**], A. V. Kotko[***], A. V. Gilchuk[*], P. Ochin[****], V. I. Kolomytsev[**], and Yu. N. Koval[**]

[*]*National Technical University of Ukraine 'Kyiv Polytechnic Institute', 37 Peremogy Prospekt, UA-03506 Kyiv, Ukraine*
[**]*G. V. Kurdyumov Institute for Metal Physics, N.A.S. of Ukraine, 36 Academician Vernadsky Blvd., UA-03680 Kyiv-142, Ukraine*
[***]*I. M. Frantsevich Institute for Materials Science, N.A.S. of Ukraine, 3 Krzhizhanovskyi Str., UA-03680 Kyiv-142, Ukraine*
[****]*Institut de Chimie et des Matériaux Paris Est (ICMPE–CNRS), 2–8 Henri Dunant Rue, 94320 Thiais, France*

The microstructure of Cu–13.0Al–3.9Ni–0.4Ti–0.2Cr wt.% compacts sintered by spark plasma method from powders prepared by spark-erosion method in liquid argon from master alloy is investigated. Powder is annealed in H_2 atmosphere before the spark plasma sintering. SEM and TEM investigations reveal that sintered samples have a composite structure, which consists of the micron and submicron spherical metallic particles embedded into the binder matrix. This matrix seems to be the product of copper oxide reduction according to the scheme $CuO \rightarrow Cu_4O_3 \rightarrow Cu_2O \rightarrow Cu_8O$ and aluminium hydroxides' conversion according to the flowchart aluminium hydroxide $\rightarrow$ transition alumina $\rightarrow \alpha$-Al_2O_3, during the annealing and/or sintering. TEM study reveals that main phase in metallic particles is self-accommodated 18R martensite. The regular basal plane stacking faults and/or $(001)_{18R}$ microtwins are dominant defects in 18R martensite. 18R martensite of single orientation occupies entire volume of spherical nanoparticles, being the basal plane stacking faults and/or $(001)_{18R}$ microtwins, which have different thicknesses.

Досліджено мікроструктуру компактів Cu–13,0Al–3,9Ni–0,4Ti–0,2Cr ваг.% спечених плазмово-іскровим методом із електроерозійних порошків, виготовлених із мастер-стопу в рідкому арґоні. Перед спіканням по-

рошок відпалювався в атмосфері водню. Спечені зразки мають композитну структуру, що утворена із мікронних і субмікронних сферичних металевих частинок, вбудованих у зв'язувальну матрицю. Остання є результатом відновлення під час відпалу та/або спікання оксиду міді відповідно до схеми $CuO \rightarrow Cu_4O_3 \rightarrow Cu_2O \rightarrow Cu_8O$ та гідроксидів алюмінію згідно зі схемою гідроксид алюмінію → перехідний окис алюмінію → α-Al_2O_3. Встановлено, що основною фазою в металевих частинках є самоузгоджений багатоваріянтний 18R-мартенсит, домінантні дефекти якого є реґулярними дефектами пакування в базовій площині та/або $(001)_{18R}$-мікродвійники. Весь об'єм сферичних наночастинок займає одноваріянтний 18R-мартенсит; при цьому дефекти пакування в базовій площині та/або $(001)_{18R}$-мікродвійники мають різні товщини.

Исследована микроструктура компактов Cu–13,0Al–3,9Ni–0,4Ti–0,2Cr масс.%, спечённых плазменно-искровым методом из электроэрозионных порошков, изготовленных из мастер-сплава в жидком аргоне. Перед спеканием порошок отжигался в атмосфере водорода. Спечённые образцы имеют композитную структуру, которая состоит из микронных и субмикронных сферических металлических частиц, встроенных в связующую матрицу. Последняя является результатом восстановления при отжиге и/или спекании оксида меди согласно схеме $CuO \rightarrow Cu_4O_3 \rightarrow Cu_2O \rightarrow Cu_8O$ и гидроксидов алюминия согласно схеме гидроксид алюминия → переходный оксид алюминия → α-Al_2O_3. Установлено, что основной фазой в металлических частицах является самосогласованный многовариантный 18R-мартенсит, доминантными дефектами которого являются регулярные дефекты упаковки в базовой плоскости и/или $(001)_{18R}$-микродвойники. Весь объём сферических наночастиц занимает одновариантный 18R-мартенсит; при этом дефекты упаковки в базовой плоскости и/или $(001)_{18R}$-микродвойники имеют разные толщины.

Key words: 18R martensite, basal plane stacking faults, microtwins, Cu–Al–Ni alloys, spark plasma sintering method, spark-erosion method.

(Received November 28, 2013; in final version, July 07, 2014)

1. INTRODUCTION

Cu–Al–Ni alloys are being developed as ones of the alternatives for the intermediate temperature application. Polycrystalline Cu–Al–Ni alloys produced by conventional casting method are quite brittle [1], due to their very high elastic anisotropy ($A \cong 13$), large grain size and strong orientation dependence of transformation strain [2, 3]. Among other methods, which refine the substructure, the powder metallurgy route is a good alternative for near-net shape alloy products with a better control of the grain sizes.

The operation with pre-alloyed powders has an unambiguous feedback caused by the solid-state diffusion mechanism of powder sintering. The processes of the decomposition, precipitating and ordering

superimposing on the sintering processes can modify the characteristics of the martensitic transformation (MT). Therefore, the spark plasma sintering (SPS) method looks as a promising one-step process alternative to the conventional sintering of pre-alloyed powders. In our previous work [4], massive Cu–13.01Al–3.91Ni–0.37Ti–0.24Cr wt.% shape memory alloy was synthesized by the spark plasma sintering method from pre-alloyed powder prepared by the spark-erosion method (SE) in liquid argon. XRD, EDS, Auger microanalyses showed that the composite structure of spark-plasma sintered compacts appears due to the interaction between Al and CuO oxide from superficial layers of submicron particles as well as nanofractions of powder. It could cause the reduction of CuO oxide to Cu_2O oxide and promote good sintering of material even at low temperature of sintering. In addition, the martensitic phase in the sintered compacts has been clearly indicated by SEM and XRD study. However, smallest scales of the microstructure of sintered compacts are not studied.

The aim of current work is to elucidate the peculiarities of microstructure of the spark-plasma sintered composite and to reveal the martensite microstructure of Cu–Al–Ni particles of different scales embedded in extrinsic matrix.

2. EXPERIMENTAL

Hot-rolled rods of Cu–13.01Al–3.91Ni–0.37Ti–0.24Cr wt.% were produced by AMT (Belgium). The rods were annealed 30 min at 800°C followed by water quenching. Part of the rods were used as electrodes for SE apparatus and the remaining were broken in 3–4 mm pieces and were used to obtain powder by spark erosion method. The general principle of the spark-erosion processing is described in details in [5].

The SPS apparatus DR.SINTER® LAB Series is used for sintering. Uniaxial pressure of maximum 99.5 MPa is applied for densification. About 1 g of powder was preliminary slightly compacted in the die, placed inside the working chamber and the system was evacuated. As a result, the compacts with a diameter of 8 mm and height of 4–6 mm were obtained.

XRD study of the powder and compacts is carried out at room temperature in Bragg–Brentano configuration with a Co$K_{\alpha 1,2}$-radiation. A PANalyticalX'Pert PRO diffractometer with a linear detector is used. The morphology and composition study of the sintered samples is analysed by JSM-6490LV or Auger spectrometer JAMP-9500F both equipped with EDX spectrometer INCA PentaFETx3. Specimens are etched by Ar^+ ions before the inspection. TEM investigation is carried out with JEOL 100CX operating under accelerating voltage 100 kV. Samples for the TEM investigation are prepared by the dimpling of 3 mm diameter specimens followed by Ar^+ ions etching.

3. RESULTS AND DISCUSSION

3.1. Phase Content and Microstructure of Sintered Samples

XRD patterns (Fig. 1, *a*) have shown that, as-obtained powder contains mainly β_3 ($L2_1$) phase, γ' (2H) martensite phase, copper oxide CuO (tenorite); one minute peak can be attributed to Cu. The width of CuO peaks is large, thus one can assume that they relate with the nanoparticles of CuO, which appeared due to the reaction with residue of oxygen in liquid argon as well as during the storage. After annealing in hydrogen, CuO peaks have disappeared completely, instead of them peaks of Cu_2O (ISCD # 75-1531, cuprite) have appeared. In addition, distinct peaks of γ_2 (Cu_9Al_4) were found. After spark plasma sintering processing, the intensity of β_3 and γ_2 peaks as well as those of γ' martensite has diminished dramatically; instead of them peaks of β' (18R) phase have appeared.

SEM investigation revealed that after the sintering of spark erosion powder annealed in H_2 atmosphere, the structure is a composite (Fig. 1, *b*). It consists of the micron and submicron metallic spherical particles with the compositions close to the master alloys. They are embedded into the matrix, which seems to be mixture of Al and Cu oxides derived from the nanofraction of spark erosion powder. This result has been already reported elsewhere in details [4, 6].

SEM examinations of Ar^+ ions etched samples revealed also that boundaries of the particles as well as interspacing between them (binder fraction) were less etched in comparison with the body of metallic particles. As a result, the etched particles look as decorated by thin perhaps ceramic walls.

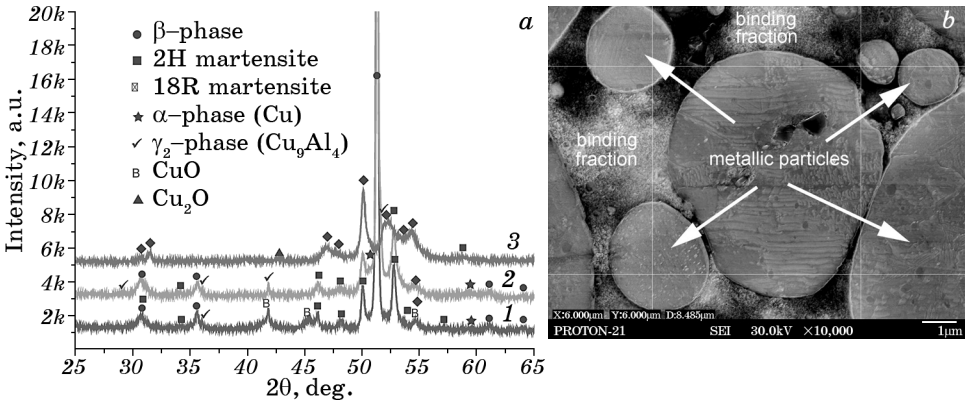

Fig. 1. *a*—XRD spectra of as received powder (*1*), powder annealed in H_2 at 290°C for 1 hour (*2*), spark plasma sintered sample (*3*); *b*—SEM of Ar^+ ion etched spark plasma sintered sample.

3.2. Chemical Composition and Structure of the Binder (Ceramic) Fraction

TEM investigation has confirmed that the binder fraction that fills the interspaces between the spherical micron-size particles is the complex mixture of the oxides. The diffusive and spotted rings, which appeared on the electron-diffraction patterns taken from different loci of the samples, indicate the different sizes of the binder components (Fig. 2). Some of them clearly appeared on the SAED taken from the segments of the rings (Fig. 2). The surface layer on the micron sized particles with the typical width 10–30 nm is clearly seen too on dark field images (Fig. 2). It gives evidence that this layer is also some kind of oxides. The calculated interplanar spacings are grouped in several clusters, only five of them are presented on all patterns; others appear only on certain electron-diffraction patterns. Moreover, the interplanar spacings inside each of groups are slightly different, but these differences are out of the instrumental error. All this points out that structure of the binder phase is inhomogeneous and consists of the different kinds of oxides.

Among the possible candidates, the following is the most relevant as regards the relative intensity of the reflexes. There are the sets of copper oxides: cuprite Cu_2O with cubic symmetry (space group $Pn\bar{3}m$), paramelaconite Cu_4O_3 [7] with tetragonal symmetry (group $I4_1/amd$), and possible one of the cooper suboxides Cu_8O [8] with orthorhombic symmetry (space group $Bmm2$). Although some of the reflexes on the rings are well fitted by the reflexes of the monoclinic CuO (tenorite), its presence in the binder is unlikely, as its strongest reflexes are not found. Other set of oxides are the aluminium oxides. Except the stable α-Al_2O_3 (corundum), most of the transition aluminas [9] cannot be excluded. Some of them with cubic symmetry are preferable since specif-

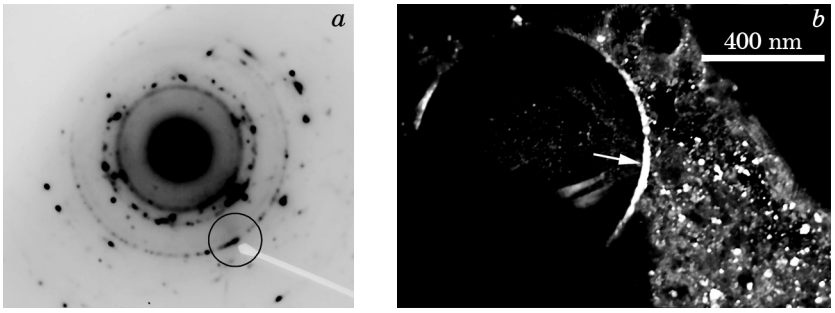

Fig. 2. Microstructure of the binding fraction. *a*—diffraction pattern, circle indicates the area on the ring, from where the DF image was made; *b*—DF image of the binding fraction. Arrow indicates the interfacial layer on the micron sized particle with martensite plates inside.

ic relations between the interplanar spacing have been observed. Namely, χ-alumina [9], γ-alumina [9, 10] with the composition $Al_{2.67}O_4$ (other name σ-alumina with spinel-type structure and composition close to $Al_{2.667}O_4$ [11]), η-alumina with the composition close to the stoichiometric $Al_{21.333}O_{32}$ [9, 12] both belonging to the space group $Fd\bar{3}m$. Finally, the reflexes of copper–nickel aluminates spinel [13] $Cu_xNi_{1-x}Al_2O_4$ (space group $Fd\bar{3}m$) also good fit the spots on the rings.

3.3. Binder Fraction Formation Mechanism

In spite of the lack of certainty in the phase composition of the binder as well as the interfacial layer of particles, the above-proposed sets of oxides are plausible. These collections seem to be the result of feasible scenarios of the transformations between the different type of oxides and Cu–Al–Ni particles during the preliminary ageing followed by spark plasma sintering. To explain the transformation of CuO oxide into Cu_2O oxide and large heat release, which has been observed at 900°C during the heating of powder, the redox reactions between the CuO oxide and Al in as-prepared powder has been proposed in [4, 6]. Current TEM investigation has shown that there are several scenarios of such transformations, which could be fulfilled during the heat treatments of powder.

The scheme of copper oxide reduction is the following: $CuO \rightarrow Cu_4O_3 \rightarrow Cu_2O \rightarrow Cu_8O \rightarrow Cu$. It seems that the last stage in this chain is absent. The metastable suboxide Cu_8O has the unit-cell volume approximately four times larger than that of Cu_20 and it is usually formed on early stage of copper oxidation [8]. However, one cannot exclude the reverse transformation under appropriate conditions, namely the heating in reduction atmosphere (H_2) or in the presence of the elements with greater affinity to oxygen like aluminium. According to [7], the Cu_4O_3 paramelaconit structure can be described either as derived from the CuO structure by ordered removal of oxygen atoms, or as derived from the Cu_2O structure by ordered insertion of oxygen atom. Thus, this is the intermediate form between tenorite and cuprite. The reduction of initial form of copper oxide is terminated on the different steps of the above-mentioned sequence, depending on the local surrounding and other conditions affecting the oxygen transport.

According to Ellingham diagram, the reduction of tenorite in hydrogen atmosphere has been favourable energetically, independently on the temperature. On the other hand, the Al presence enhances this process owing the movement of oxygen atoms from copper oxides toward the aluminium atoms, which have bigger affinity to oxygen. Aluminium atoms are present in the powder in two fractions: in nanofraction, which is formed due to the condensation of vapour phase during spark erosion, and in the micron-size Cu–Al–Ni particles.

It is hard to believe that aluminium exists in oxygen-free state in nanofraction due to high affinity of aluminium to oxygen. It also has not been found in state of suboxide AlO and Al_2O [14]. More plausible that aluminium appears in the nanofraction in various forms of aluminium trihydroxides $Al(OH)_3$ (gibbsite, bayerite, nordstrandite) and/or aluminium oxide hydroxides AlO(OH) (boehmite, diaspore). These hydroxides are converted during the annealing and/or sintering into various forms of alumina according to the flowchart: aluminium hydroxide → transition aluminas → α-Al_20_3 [15]. According to the flowchart [15], in the temperature interval between 300 and 700°C, the most likely outcome is the transformations into χ-, η- and γ-alumina depending on the initial forms of hydroxides and temperature.

There is another attractor for the oxygen atoms, namely, aluminium atoms on the surface of micron-size particles. Naturally, in that case the copper–nickel aluminate spinel $Cu_xNi_{1-x}Al_2O_4$, which is isomorphous to the η-, γ- and χ-alumina, and have similar lattice parameter is formed on the surface of Cu–Al–Ni particles during the heat treatments.

3.4. Microstructure of the Micron-, Submicron- and Nanoparticles

TEM investigation of metallic spherical particles reveals several peculiarities. All particles embedded in ceramic binding phase are in martensite state, at least those ones with the dimension more than 100 nm. That fact is easily manifested under appropriate conditions such as needle-like or banded structures inside the particles. Only submicron and nanosize particles appear as the disks decorated by superficial layer. Larger ones look as grains with irregular curved boundaries that seem to be related to nonuniform conditions during the $\underline{A}r^+$ etching.

The self-accommodated 18R martensite plates in (128) twin related orientations, which occupy the relatively large particle (of size about 1 μm) with irregular boundaries, are shown in Fig. 3. The microstruc-

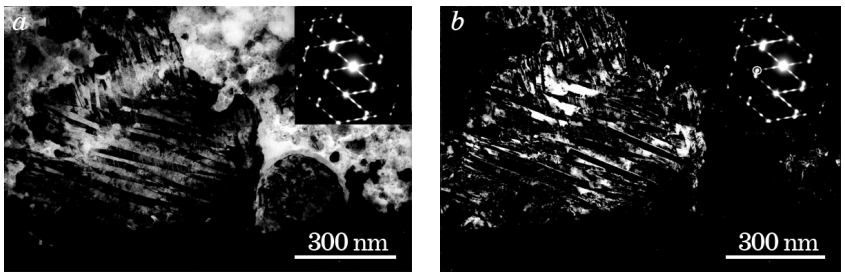

Fig. 3. Microstructure of 18R martensite in the micron sized particle. Diffraction pattern is presented on inset. Zone axis is [210]. BF image (*a*); DF image (*b*). Circle indicates the spot, from where the DF image is taken.

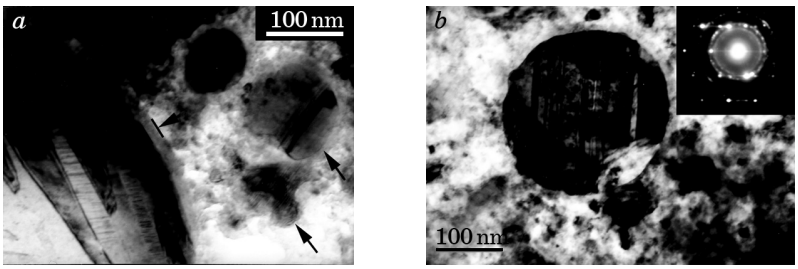

Fig. 4. Microstructure of the smallest particles. *a*—micron sized and two nanosize particles. Calliper indicates the superficial layer on large particle. Arrows indicate the strip contrast in smallest particles; *b*—BF image of the nanosize particle. Diffraction pattern is presented on inset. Zone axis is approximately [210].

ture of those crystals consists of typical for Cu–Al–Ni basal plane stacking faults. Somewhere, the (001) 18R microtwins have been observed. This observation well correlates with the HRTEM investigation of 18R martensite in Cu–Al alloy [16]. The neighbouring practically spherical particles sized 300 nm are out of good diffraction conditions.

It is interesting that the smallest particles sized 100–200 nm appear with striped contrast (Fig. 4, *a*). It supposed that martensite of only one variant occupies entire volume of nanosize particle. Because of their small dimension and adjacent particles in other orientations, it is very difficult to get good diffraction pattern as well as SAED to reveal the microstructure of such kind of particles. The rare event under more or less suitable experimental conditions is presented in Fig. 4, *b*. The nanosize particles with (001) 18R microtwins or basal plane stacking faults occupy entire volume of particles; no martensite plates or accommodation groups of martensite are seen. Similar microstructure of martensite has be observed by T. Waitz *et al.* [17] in nanosize grains after isothermal annealing of high-pressure torsion deformed amorphous Ni–50.3 at.% Ti as well as in NiTi nanocrystals embedded into the amorphous matrix [18]. Other peculiarity is that the width of microtwins (or stacking faults) is different and their appearing is irregular.

4. CONCLUSIONS

The microstructure of SPS Cu–13.0Al–3.9Ni–0.4Ti–0.2Cr wt.% compacts sintered from the SE powders prepared in liquid argon consists of the micron and submicron spherical metallic particles embedded into the binder matrix. This matrix can be considered as the product of copper oxide reduction ($CuO \rightarrow Cu_4O_3 \rightarrow Cu_2O \rightarrow Cu_8O$) and aluminium hy-

droxides conversion (aluminium hydroxide → transition aluminas → α-Al_2O_3) during the annealing in H_2 atmosphere and/or sintering. The superficial layer in metallic powder seems to be the copper–nickel aluminates spinel $Cu_xNi_{1-x}Al_2O_4$. Basic phase in metallic particles is 18R martensite. The dominant defects are the regular basal plane stacking faults and/or (001) 18R microtwins. 18R martensite of single orientation occupies entire volume of spherical nanoparticles, being the basal plane stacking faults and/or (001) 18R microtwins, which have different thicknesses.

ACKNOWLEDGEMENTS

Authors appreciate Prof. G. S. Oliynyk for the consultation and assistance in the Ar^+ ions etching of the SPS samples for TEM investigation.

REFERENCES

1. S. Miyazaki, K. Otsuka, H. Sakamoto, and K. Shimizu, *Trans. Jpn. Inst. Met.*, **4**: 244 (1981).
2. S. Miyazaki and K. Otsuka, *Shape Memory. Alloys, Precision Machinery and Robotics* (Ed. H. Funakubo) (New York: Gordon and Breach: 1987), vol. **1**, p. 116.
3. S. Miyazaki and K. Otsuka, *ISIJ Int.*, **29**: 353 (1989).
4. R. A. Portier, P. Ochin, A. Pasko, G. E. Monastyrsky, A. V. Gilchuk, V. I. Kolomytsev, and Yu. N. Koval, *J. Alloys Compd.*, **577**, Suppl. 1: S472 (2013).
5. J. Carrey, H. B. Radousky, and A. E. Berkowitz, *J. Appl. Phys.*, **95**: 823 (2004).
6. G. E. Monastyrsky, P. Ochin, A. V. Gilchuk, V. I. Kolomytsev, and Yu. N. Koval, *J. Nano- Electron. Phys.*, **4**: 01007-1 (2012).
7. M. O'Keeffe and J. O. Bovin, *American Mineralogist*, **63**: 180 (1978).
8. R. Guan, H. Hashimoto, and K. H. Kuo, *Acta Cryst.*, **B40**: 560 (1984).
9. P. S. Santos, H. S. Santos, and S. P. Toledo, *Materials Research*, **3**: 104 (2000).
10. L. Smrcok, V. Langer, and J. Krestan, *Acta Crystallogr.*, **C62**: i83 (2006).
11. W. Guse and H. Saalfeld, *Neues Jahrbuch für Mineralogie Monatshefte*, **5**: 217 (1990).
12. Yo. K. Shi, *J. Ceram. Soc. Jpn.*, **84**: 610 (1976).
13. C. O. Areán and J. S. D. Vicuela, *J. Solid State Chem.*, **60**, Iss. 1: 1 (1985).
14. M. Hoch and H. L. Johnston, *J. Am. Chem. Soc.*, **76**, No. 10: 2560 (1954).
15. *Industrial Alumina Chemicals. ACS Monograph 184* (Ed. C. Misra) (Washington, DC: American Chemical Society: 1986), p. 76.
16. F. Lovey, G. Van Tendeloo, G. Van Landuyt, and S. Amelinckx, *Scr. Met.*, **19**, No. 10: 1223 (1985).
17. T. Waitz, V. Kazykhanov, and H. P. Karnthaler, *Acta Mater.*, **52**: 137 (2004).
18. T. Waitz and H. P. Karnthaler, *Acta Mater.*, **52**: 5461 (2004).